INSTITUTE OF PHYSICS PUBLISHING MODELLING AND SIMULATION IN MATERIALS SCIENCE AND ENGINEERING

Modelling Simul. Mater. Sci. Eng. **14** (2006) S55–S62 doi:10.1088/0965-0393/14/5/S07

Atomistic simulations of elastic deformation and dislocation nucleation in Al under indentation-induced stress distribution

Tomohito Tsuru[1] **and Yoji Shibutani**[1,2]

[1]Department of Mechanical Engineering, Graduate School of Engineering, Osaka University, 2-1, Yamadaoka, Suita, Osaka, 565-0871, Japan
[2] Center for Atomic and Molecular Technologies, Osaka University, 2-1, Yamadaoka, Suita, Osaka, 565-0871, Japan

E-mail: tsuru@comec.mech.eng.osaka-u.ac.jp

Received 20 September 2005, in final form 23 December 2005
Published 26 May 2006
Online at stacks.iop.org/MSMSE/14/S55

Abstract

Preliminary simulations of simple shear deformation and indentation simulations using different radii of a spherical indenter are performed using molecular dynamics in order to uncover the internal stress state for elastic deformation and subsequent initial plasticity under nano-indentation. An atomic single-crystalline aluminium model containing up to 1,372,000 atoms and an ideal friction-free spherical indenter are presented in a set of simulations. Effects of the stress distribution using several kinds of spherical radii of indenters on the critical condition of dislocation emissions are discussed with much emphasis. The critical shear stress for the dislocation emission under indentation is well accorded with the shear strength under the simple shear deformation exposed to the equivalent external stresses to the indentation-induced stress states. It is confirmed that shear strength strongly depends on the external stress component and therefore, high compressive stress states generated beneath the indenter lead to the much higher critical shear stress than $\mu/2\pi$.

(Some figures in this article are in colour only in the electronic version)

1. Introduction

Recent advances in material miniaturization techniques have allowed for the use of microscale materials in various structures, such as integrated circuits and microelectromechanical systems (MEMS). It is well known that the motion of dislocations and their collective behaviour play an important role in the properties of these microscale materials. The indentation technique has been extensively used to measure the hardness and other nano-scaled properties of materials [1].

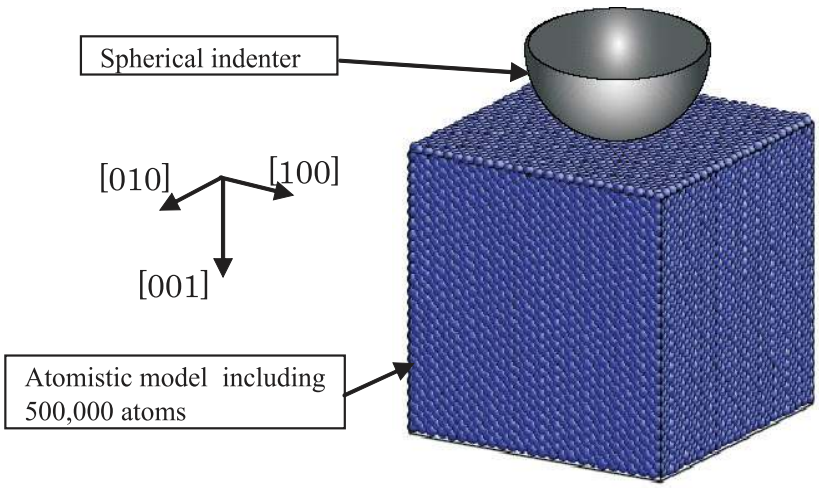

Figure 1. Atomistic model of single-crystalline aluminum indented by a spherical indenter.

Recently, an unstable displacement burst has been observed in the relationship between the indent load and indent depth in the nano-indentation experiment [2–4]. A number of straightforward atomistic simulations [5–7] and large scale quasi-continuum simulations of a more realistic indenter size [8] have been performed so far. However, the cause of the abrupt displacement burst is still a controversial topic. For single-crystal materials, the first event of nano-plasticity occurs when maximum shear stress generated under the indenter is on the order of the theoretical shear strength [1]. On the other hand, recent first-principle calculations of simple shear deformation indicate that the ideal shear strength strongly depends on the external stresses whose effects differ according to the materials [9]. Therefore, it will be an intractable problem to present rigorous criterion of the critical state for dislocation nucleation. In the present paper, the ideal shear strengths of single-crystalline aluminium under the different direction and magnitude of external stress conditions are calculated using an empirical interatomic potential. And then using the same potential, the nano-indentation process in single-crystalline aluminium is simulated using the molecular dynamics (MD) simulations in order to comprehend the critical state under nano-indentation and the mechanism of dislocation emission.

2. Analysis model

An atomistic model containing 500,000 or 1,372,000 atoms of single-crystalline aluminium which is a cube of (20 nm × 20 nm × 20 nm) or (28 nm × 28 nm × 28 nm) aligned along [100], [010] and [001] directions as well as an ideal friction-free spherical indenter were used as shown in figure 1. The material is indented with four different radii (r5 nm, r15 nm, r20 nm, r30 nm) of spherical indenters. A large-scale model is used in the case of the r30 nm indentation. The top surface oriented along the [001] direction is traction-free and the atoms located on the bottom surface are absolutely fixed. Periodic boundary conditions are applied in the direction perpendicular to the indentation axis. An EAM-type interatomic potential proposed by Mishin *et al* [10] is employed in order to express the interaction between Al atoms, and the repulsive potential by Kelchner is chosen to describe the interaction between

Table 1. Mechanical properties of single-crystalline aluminum obtained by the Mishin potential: the lattice constant a_0, $\{111\}\langle 11\bar{2}\rangle$ directional shear modulus G', unstable stacking fault energy γ_{us} and stacking fault energy γ_{SF}.

	Al	
Properties	Mishin	DFT[a]
a_0 (Å)	4.05	4.04
G'(GPa)	27.9	25.4
γ_{us} (mJ m^{-2})	189.7	175
γ_{SF} (mJ m^{-2})	156.6	158

a [6]

the indenter and material [5, 6]. The MD simulations are performed as quasi-static analysis under the absolute 0 K temperature by the conjugate gradient method (CG). The indent load is applied by a small indent depth of ∼0.25 Å and a fully relaxed condition is obtained after 4000–6000 CG steps. A set of calculations is repeated until the indent depth reaches the maximum depth: h_{max} = 15 Å. In table 1, we show the physical properties of aluminium predicted by the Mishin potential. The advantage of using the Mishin potential will be discussed in the following section.

3. Ideal shear strength under external stress in aluminium

Preliminary simulations of simple shear deformation were performed in order to investigate the effect of the external stress on the ideal shear strength in single-crystalline aluminium. The analysis model along the direction of $x[1\bar{1}0]$, $y[11\bar{2}]$and $z[111]$ is given and $(111)[11\bar{2}]$ directional pure shear deformations are applied under the various kinds of external normal stresses controlled by a cell control method [11]. The relationship between stress and displacement normalized by the magnitude of a partial dislocation in the unrelaxed condition is shown in figure 2, and maximum shear stresses under various external stresses are shown in table 2. For comparison, the case of single-crystalline copper is also presented in this figure and table. It can be seen in figure 2 that all the normal stress components arise in the process of shear deformation. The relaxed maximum shear stress, which can be calculated by the full relaxation of these normal stress components, is also indicated in table 2. In spite of the lower $\{111\}\langle 11\bar{2}\rangle$ shear modulus and unrelaxed maximum stress in aluminium, the relaxed maximum stress is higher than that in copper. This particular feature is caused by directional bonds in aluminium as determined using DFT calculations [9]. While it has been difficult to present these anomalous features of aluminium using EAM-type potential, the Mishin potential overcomes problems associated with directional bonds. Further discussion about directional bond is beyond the scope of this paper. It is, however, of considerable significance that the maximum shear stress strongly depends on both direction and magnitude of the external stress.

4. Results and discussion

4.1. Indent load and mean pressure

The relationship between indent load and mean pressure as a function of the indent depth during the nano-indentation process using different radii of a spherical indenter is depicted in figure 3. In this figure, the mean pressure p_m is defined as the following equation:

$$p_m = P/A_c.$$

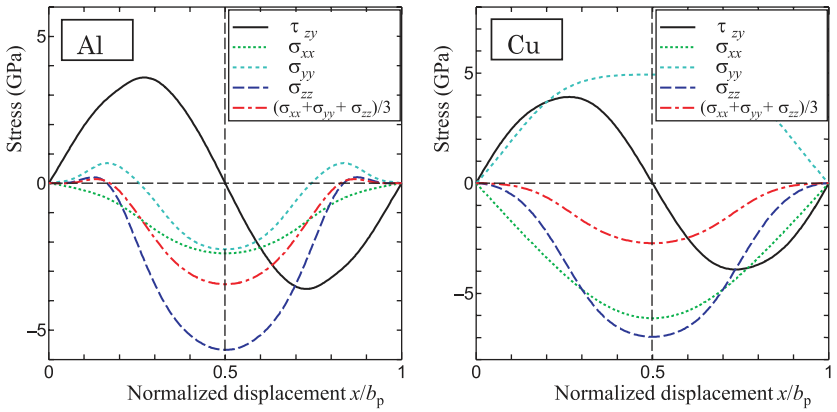

Figure 2. Stress-displacement response in Al and Cu.

Table 2. Maximum shear stress under external loading.

	Ideal shear strength (GPa)	
External stress (GPa)	Al	Cu
Unrelax	3.60	3.91
Relax	3.19	2.86
$(\sigma_{xx}+\sigma_{yy}+\sigma_{zz})/3 = -5.0$	4.86	3.45
$(\sigma_{xx}+\sigma_{yy}+\sigma_{zz})/3 = 5.0$	1.85	2.37
$\sigma_{xx} = -2.5$	2.92	3.09
$\sigma_{xx} = 2.5$	3.47	2.31
$\sigma_{yy} = -2.5$	3.54	2.55
$\sigma_{yy} = 2.5$	2.99	3.06
$\sigma_{xx} = \sigma_{yy} = -2.5$	3.22	2.91
$\sigma_{xx} = \sigma_{yy} = 2.5$	3.18	2.75
$\sigma_{zz} = -2.5$	3.88	2.94
$\sigma_{zz} = 2.5$	2.41	2.68

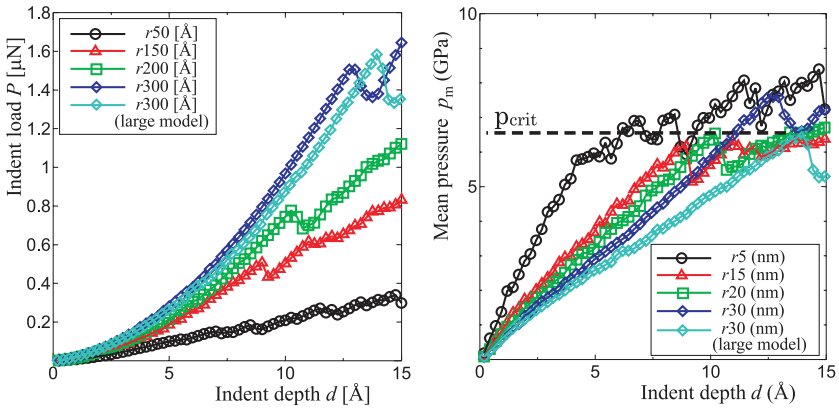

Figure 3. Relationship between indent load, mean pressure and indent depth.

Here, A_c is the contact area which is directly calculated within the simulation. After the elastic increase of the indent load, an abrupt load drop which is related to the displacement burst in a nano-indentation experiment is observed in figure 3(*a*). This load drop implies dislocation nucleation. A similar drop is also observed in figure 3(*b*) and the values of the critical mean pressure p_{crit} are almost the same except for the $r30$ nm indenter. In the case of the $r30$ nm indenter, the boundary condition affects the properties of the whole system due to the simulation cell size. Therefore, we simulated a large-scale model containing 1,372,000 atoms indented by the $r30$ indenter and the results are also shown in figure 3. Compared with the small model, the critical mean pressure is almost the same as for other indenters. Thus, the critical mean pressure can be readily obtained from figure 3(*b*) and $p_{crit} = 6.4$ GPa. In a nano-indentation experiment, the critical resolved shear stress is generally evaluated by combining these critical values of the indent load or mean pressure and the Hertzian elastic solution as follows [12]:

$$p_{max} = \frac{3P}{2\pi a^2} = \left(\frac{6PE^{*2}}{\pi^3 R^2}\right)^{\frac{1}{3}} = \frac{3}{2}p_m, \qquad \tau_{max} = 0.31\,p_{max} = 0.31\left(\frac{6PE^{*2}}{\pi^3 R^2}\right)^{\frac{1}{3}} = 0.465\,p_m.$$

Substituting the obtained critical pressure into the above Hertzian solution, the critical shear stress τ_{crit} was estimated to be 2.98 GPa, which is of a similar order to the ideal shear strength in aluminium. As a consequence of the above mentioned procedure, it has so far been said that dislocation nucleation occurs when the resolved shear stress reaches the ideal shear strength.

In addition, it is found in figure 3(*a*) that the larger radius of the spherical indenter produces a significant load drop. This difference is caused by the configuration of emitted dislocations as described in the following section.

4.2. Dislocation emission in aluminium by different radii of spherical indenters

Overviews of dislocation emissions under nano-indentation by spherical indenters with four different radii achieved by the MD simulations are shown in figure 4, where these figures are visualized by the atomeye program [13]. We extracted the defect structures on the basis of a potential energy criterion specifying only those atoms with an energy above -3.33 eV. A prismatic dislocation loop (PDL) is observed in figure 6(*a*). The formation mechanism of a PDL is summarized as follows [14, 15]: (i) two shear loops emitted on two different slip planes unstably interact on the $\langle 011\rangle$ line of intersection of these two planes, (ii) the screw-sides of the dislocation segment on one slip plane move to the cross-slip plane that is parallel to the other slip plane and (iii) then, two dislocation loops on the two cross-slip planes unstably interact on the $\langle 011\rangle$ line again. Though no PDL can be observed in other figures due to the restriction of the simulation model, we have confirmed that this kind of radial stress distribution, generally produced by indentation or inclusion embedded within the material, tends to form PDLs.

In addition, when a material is indented by an indenter with a larger radius, a number of dislocations are emitted within the material and a number of steps corresponding to the emitted dislocations simultaneously appear on the surface. Therefore, the presence of a large number of surface steps is thought to be the trigger for the abrupt load drop in the indent load–depth curve as shown in figure 3.

4.3. Critical shear stress under nano-indentation

The Hertzian solution is solved on the assumption that the indented materials are an ideal linear elastic body and an isotropic medium, whereas anisotropy effects in single-crystal materials should be taken into account in practical analyses. Figure 5 shows the distribution of $\{111\}\langle 11\bar{2}\rangle$

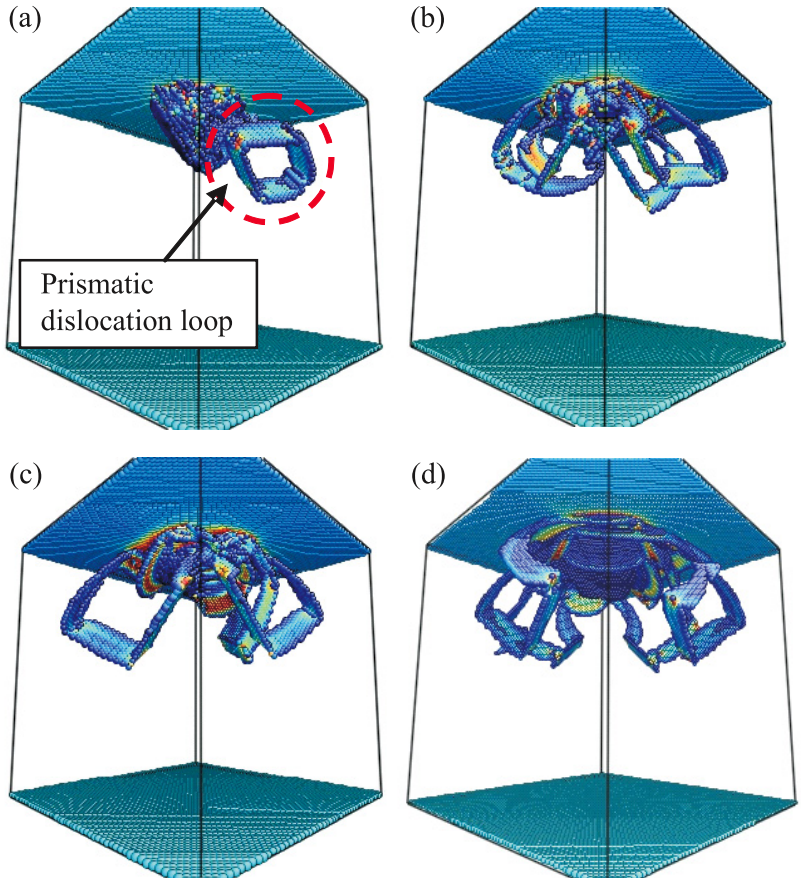

Figure 4. Dislocation emissions in aluminum indented by different radii of spherical indenters: (*a*) r 5 nm, (*b*) r 15 nm, (*c*) r 20 nm, (*d*) r 30 nm (large model).

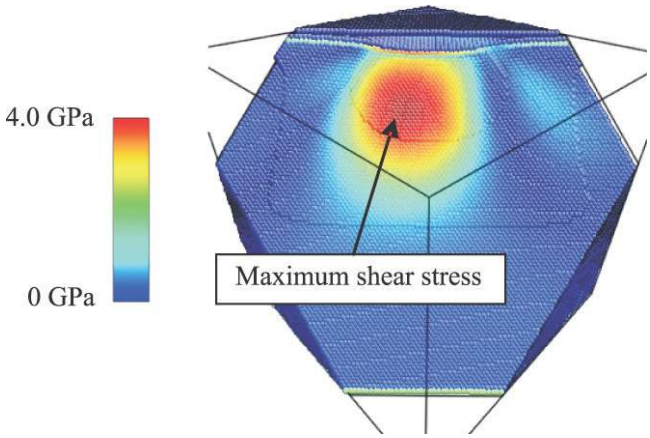

Figure 5. Distribution of $\{111\}\langle 11\bar{2}\rangle$ shear stress on the (111) plane, where the maximum shear stress occurs.

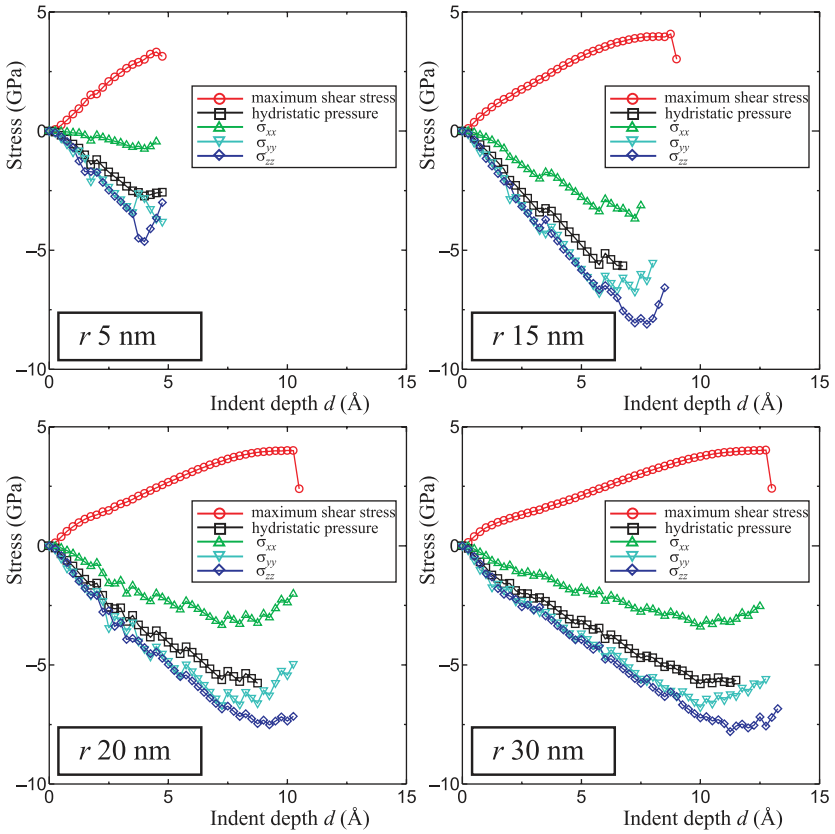

Figure 6. Normal stress and hydrostatic pressure as well as maximum $\{111\}\langle 11\bar{2}\rangle$ directional shear stress using different radii of the spherical indenter versus the indent depth.

shear stress on the (111) plane, where the atomic stress is evaluated by the Voronoi volume. It is well known from the Hertzian solution that the maximum shear stress occurs within the inner region on the indentation axis. While we can confirm that maximum stress occurs beneath the indenter, this location is slightly out of the indentation axis. This shift is related to the anisotropy of the fcc crystal. It has been indicated that a high compressive stress state is generated within the inner region beneath the indenter [16]. Therefore, we calculated the stress state within the indented material. In figure 6, the relationship between normal stress, hydrostatic pressure as well as maximum shear stress and indentation depth in the case of four different radii of spherical indenters is presented. Here, the position of the maximum shear stress can be searched within the material except for the non-fcc site using the centrosymmetry parameter [5]. This is because atoms located in the vicinity of the indenter can generate anomalous stress states. The coordinate systems are transformed from the initial coordinate system such as [001], [010], [001] into the $x[1\bar{1}0]$, $y[11\bar{2}]$, $z[111]$ coordinate system by orthogonal transformation, and then the normal stress σ_{xx}, σ_{yy}, σ_{zz}, hydrostatic pressure defined by $p = (\sigma_{xx} + \sigma_{yy} + \sigma_{zz})/3$ and $\{111\}\langle 11\bar{2}\rangle$ directional shear stress $\tau_{\max}$ can be obtained. Not to mention maximum shear stress, the magnitudes of normal stresses and hydrostatic pressure gradually increase on the compressive side with the incremental increase in indent depth. Implementing more rigorous calculations of atomic stress using the Voronoi volume, critical stresses just prior to dislocation nucleation are calculated as follows: $\tau_{\text{crit}} = 4.22\,\text{GPa}$, $\sigma_{xx} = -2.5\,\text{GPa}$, $\sigma_{yy} = -5.8\,\text{GPa}$

and $\sigma_{zz} = -7.8$ GPa. This critical shear stress is much higher than the ideal shear strength of aluminium. For confirmation, we also performed similar calculations of simple shear deformation under the same stress states ($\sigma_{xx} = -2.5$ GPa, $\sigma_{yy} = -5.8$ GPa, $\sigma_{zz} = -7.8$ GPa) as mentioned above. The maximum shear stress under these stress states was obtained to be 4.18 GPa. Consequently, considerably high compressive stress states are generated underneath the indenter and these stress states cause an elevation in the critical shear stress for dislocation emissions.

5. Conclusions

In order to investigate the internal stress state for elastic deformation and subsequent initial plasticity under nano-indentation, preliminary calculations of simple shear deformation and indentation simulations using different radii of spherical indenters were performed by MD simulations. The first simulation confirmed that the ideal shear stress is strongly affected by external stress components such as $[1\bar{1}0]$, $[11\bar{2}]$ and [111] directional normal stresses. In comparison with the Hertzian solution, anisotropy and nonlinearity within an inner region of the indented material is illustrated by atomistic simulations. In addition, the region beneath the indenter undergoes high compressive stress, and this type of high compressive stress state causes an elevation of the critical shear stress for dislocation emissions. Collective dislocation emissions and surface steps simultaneously generated are found to be a major trigger for the load drop in indentation load–depth curves.

Acknowledgments

This work was supported by the Grant-in-Aid for JSPS Fellows (179504).

References

[1] Oliver W C and Pharr G M 1992 *J. Mater. Res.* **7** 1564
[2] Suresh S, Nieh T G and Choi B W 1999 *Scr. Mater.* **41**-9 951
[3] Gouldstone A, Koh H J, Zeng K Y, Giannakopoulos A E and Suresh S 2000 *Acta Mater.* **48** 2277
[4] Shibutani Y and Koyama A 2004 *J. Mater. Res.* **19** 183
[5] Kelchner L, Plimpton S J and Hamilton J C 1998 *Phys. Rev.* B **58** 11085
[6] Zimmerman J A, Kelchner C L, Klein P A, Hamilton J C and Foiles S M 2001 *Phys. Rev. Lett.* **87** 165507-1
[7] Li J, Van Vliet K J, Zhu T, Yip S and Suresh S 2002 *Nature* **418** 307
[8] Knap J and Ortiz M 2003 *Phys. Rev. Lett*. **90** 226102
[9] Ogata S, Li J and Yip S 2002 *Science* **298** 807
[10] Mishin Y and Farkas D 1997 *Phys. Rev.* B **59** 3393
[11] Parrinello M and Rahman A 1980 *Phys. Rev. Lett.* **45** 1196
[12] Johnson K L 1985 *Contact Mechanics* (Cambridge: Cambridge University Press)
[13] Li J 2003 *Modelling. Simul. Mater. Sci. Eng.* **11** 173
[14] Shibutani Y, Koyama A and Tsuru T 2004 Solid mechanics and its applications *IUTAM Symp. on Multiscale Modeling and Characterization of Elastic-Inelastic Behaviour of Engineering Materials (Marrakech, Morocco)* **114** p 125
[15] Tsuru T and Shibutani Y 2004 Solid mechanics and its applications *IUTAM Symp. on Mesoscopic Dynamics of Fracture Process and Material Strength (Osaka, Japan)* **115** p 213
[16] Kiely J D and Houston J E 1998 *Phys. Rev.* B **57** 12588